Hindawi
Advances in Materials Science and Engineering
Volume 2024, Article ID 8895736, 12 pages
https://doi.org/10.1155/2024/8895736

Research Article

Carbonation Resistance of Cement-Based Materials Improved by Nitrite

Hao Zhang,[1,2,3,4] Luqing Cheng,[5] Jingsheng Pan,[2,3,4] Guodong Xu,[2,3,4] Xuyan Shen,[2] Song Mu,[2,3,4] Jingshun Cai,[2,3,4] Jianzhong Liu,[2,3,4] Jinxiang Hong,[2,3,4] Zhiqiang Yang,[1] Zhonglai Yi,[1] Huajian Li,[1] and Ying Zhou[2,3,4]

[1]*National Key Laboratory of High-speed Railway Track System (China Academy of Railway Sciences Group Co., LTD.), Beijing, China*
[2]*State Key Laboratory of High Performance Civil Engineering Materials, Nanjing 210008, China*
[3]*Sobute New Materials Co., LTD, Nanjing 210008, China*
[4]*Jiangsu Research Institute of Building Science, Nanjing 210008, China*
[5]*Southeast University, Nanjing 210008, China*

Correspondence should be addressed to Song Mu; musong@cnjsjk.cn

Received 12 December 2023; Revised 20 March 2024; Accepted 10 April 2024; Published 6 May 2024

Academic Editor: Sharanabasava Ganachari

Copyright © 2024 Hao Zhang et al. This is an open access article distributed under the Creative Commons Attribution License, which permits unrestricted use, distribution, and reproduction in any medium, provided the original work is properly cited.

Carbonation resistance ability is one of the most important durability-related proprieties of cement-based materials. Through the carbonation depth experiment, isothermal conduction calorimetry, XRD, BET, and water vapor sorption, the effect of calcium nitrite ($Ca(NO_3)_2$) on the carbonation properties of cement-based materials is obtained. The result indicates that the addition of $Ca(NO_3)_2$ improves the carbonation resistance property of cement-based materials if the hydration of cement pastes and microstructure is modified earlier without affecting the late hydration process. In addition, the refined pores and higher tortuosity cut down the channels, thereby impeding the ingress of carbon dioxide gas into cementitious materials, as confirmed by BET and water vapor sorption. The $Ca(NO_3)_2$ exhibits high performance in improving the carbonation resistance and extending the life of strengthened concrete.

1. Introduction

Concrete, being a primary construction material worldwide, has garnered significant academic attention regarding its structural durability [1]. Various factors in different environments influence the service life, thus affecting the durability of concrete [2]. Carbon dioxide (CO_2) erosion is one such crucial factor. Within the realm of cementitious materials, the pivotal significance of carbonation encompasses its direct influence on structural sustainability, given its potential to dismantle the passivating film on reinforcement, thereby instigating corrosion [3–5]. In the context of cementitious materials, external carbon dioxide intrudes and initiates a chemical reaction with calcium hydroxide and available water, leading to a discernible diminution of pH levels within the system, specifically descending from approximately 12.5 to below 10. The oxidation film of steel can be destroyed because of the deficiency of alkalinity, which increases the possibility of steel bar corrosion [6]. Meanwhile, other hydration products, including C-S-H gel and AFt crystals, are also prone to react with carbon dioxide [6]. The cohesion of hydration products decreases after carbonation, which leads to macroscopically visible decreased mechanical strength and increased porosity [7].

The negative impact of carbon dioxide erosion on cement is multifaceted, and the ability of carbonation resistance is closely associated with the internal pore structure of the cement matrix. The ingress of carbon dioxide acts as a fundamental prerequisite for succeeding chemical reactions during the carbonation process. Thus, the pore structure emerges as a principal determinant that governs the gas permeability and carbonation attributes of cement-

based materials. It is widely accepted that air permeability is related to the total porosity of the material [8]. The gas permeability coefficient correlates linearly with porosity coincidences for the same material [9, 10]. Bigger porosity is usually accompanied by a greater gas permeability coefficient. However, the influences of the pore size, connectivity, and tortuosity cannot be ignored. Poor pore connectivity can cut off the transmission path of carbon dioxide. The large pore tortuosity increases the resistance during the carbon dioxide transition [9].

It is evident that the carbonation resistance exhibited by cement-based materials is enhanced through the combined effects of reduced porosity, limited connectivity, and increased tortuosity. During the hydration process of cement, the aggregation of hydration products greatly affects the pore morphology and structure of concrete. Previous studies [11–13] investigating the influence of various initial solidification conditions on the pore structure have demonstrated that inadequate early curing leads to autogenous shrinkage phenomena and affects pore structure formation. Accelerating the cement hydration process is a potential source of modifying the configuration of pore structures [14, 15]. The relevant study indicates that the incorporation of a certain amount of $Ca(NO_3)_2$ into cement promotes the formation of ettringite and nitrate-containing AFm phases. Furthermore, $Ca(NO_3)_2$ accelerates the hydration of C3S [16]. $Ca(NO_3)_2$ is an accessible chemical substance that can be extracted from pond sediments and industrial wastewater [17], employing $Ca(NO_3)_2$ to enhance the performance of cement proves advantageous for sustainable development. Nevertheless, the roles of $Ca(NO_3)_2$, particularly on the carbonation resistance characteristics of concrete, have received limited attention in the literature.

This study mainly focuses on revealing how $Ca(NO_3)_2$ affects the carbonation resistance performance of cement-based materials. The investigation incorporates a combination of experimental techniques, including BET analysis, isothermal conduction calorimetry, water vapor sorption, and XRD. The findings reveal that $Ca(NO_3)_2$ and the underlying modification mechanism impart an impact on the microstructure of cementitious materials. This study offers a fresh perspective on the influence of $Ca(NO_3)_2$ modification on the pore structure during the hydration process. It establishes a theoretical foundation for the utilization of $Ca(NO_3)_2$ in enhancing the carbonation resistance of the cement matrix.

2. Methods

2.1. Experimental Materials and Preparation Process. The content of ordinary Portland cement (OPC) utilized during the investigation is presented in Table 1. The composition analysis reveals that the cement comprises 56.7 wt.% C3S, 14.3 wt.% C2S, 3.2 wt.% C3A, and 12.0 wt.% C4AF, as determined by XRD measurement. Figure 1 depicts the distribution of particle sizes present in the cement. For the experimental setup, $Ca(NO_3)_2$ of chemical grade sourced from Sigma-Aldrich Co., Ltd., is employed. The dosage of $Ca(NO_3)_2$ is varied at 1%, 2%, and 3% relative to the bulk of the cement.

Table 1: Chemical and phase composition of Portland cement.

CaO	SiO_2	Al_2O_3	SO_2	Fe_2O_3	MgO	K_2O	TiO_2	Na_2O
62.714	19.191	4.446	2.362	3.16	1.941	0.453	0.329	0.183

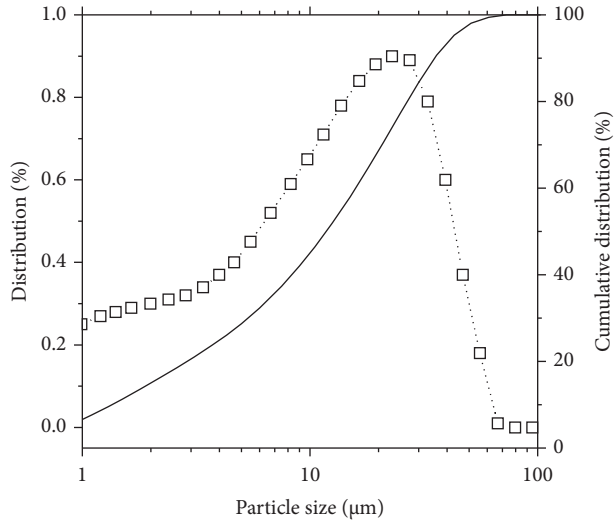

Figure 1: The particle size distribution of cement.

The experimental procedure involved the utilization of OPC to fabricate cement paste specimens with a prescribed 0.4 water-to-cement ratio. The dimensions of the samples were set at $40 \times 40 \times 160\ mm^3$. To prevent carbonation, a plastic film was used to demold the cement paste samples after 1 day. Subsequently, the specimens were subjected to a curing process for 28 days in a dedicated curing room. Following the guidelines stated in Chinese standard GB/T 17671-2021, a concrete specimen measuring $100\ mm \times 100\ mm \times 400\ mm$ in dimensions was fabricated as the subjected sample for the accelerated carbonation experiment. The demolding process was executed 24 hours after casting, followed by a curing period that extended until 28 days. Keep the temperature at 20°C, relative humidity at 95% during the curing process. Table 2 presents the mixture design of concrete samples, which will be used in this experiment.

2.2. Accelerated Carbonation and Mechanical Strength. To reduce saturation before initiating accelerated carbonation, the samples were dried at 60°C for 48 hours. Subsequently, the specimens were relocated to the carbonation chamber for specific durations of 28, 56, 90, and 180 days. In compliance with the Chinese durability, criterion GB50082-2009 meticulously controlled to create specific environmental conditions. The carbonation chamber maintained a consistent temperature of 20°C, while the relative humidity was carefully regulated at 70%. Additionally, the CO_2 concentration within the sample storage chamber was set at 20%. After subjecting the samples to carbonation experiments for the specified duration, applying a 1% phenolphthalein alcohol solution using a spray method, then measure the carbonation depth. Use a hydraulic press to test the

Table 2: Mixture design of concrete used in the study.

W/C	Cement (kg/m^3)	Coarse aggregate (kg/m^3)	Fine aggregate (kg/m^3)	Sand (kg/m^3)	Water (kg/m^3)
0.5	350	642.5	430	777	175

mechanical properties of the test block before the carbonization process, and obtain the compressive strength data of the test block.

2.3. Characterization Experiment

2.3.1. Isothermal Calorimetry. With the aim of investigating the influence of $Ca(NO_3)_2$ on the process of hydration, we use a TAM air isothermal calorimeter to measure the isothermal calorimetry. A quantity of approximately 5 g of cement paste was measured and subsequently placed within a polyethene container. The obtained results were appropriately adjusted based on the mass of the cement sample.

2.3.2. X-Ray Diffraction (XRD). To determine the composition of the hydration phases in the respective samples, the samples were ground until they formed a fine powder. Subsequently, the powdered samples were sifted through an 200-mesh sieve to ensure uniformity in particle size. The X-ray diffraction was performed in the angle range of 5–70°with a time interval of 0.45 seconds each step utilizing the D8 Advance diffractometer, manufactured by Bruker in Germany. The Rietveld method, implemented through the utilization of TOPAS software, was employed to quantitatively determine the proportion of each phase present following the hydration process.

2.3.3. Specific Surface Area and Porosimetry (BET). To investigate the alterations in the pore structure resulting from the influence of $Ca(NO_3)_2$, a Micro TriStar II 3flex surface analyzer (model: 3 Flex, manufactured in the USA) was employed. The samples were degassed in vacuum for 24 hours at a constant temperature of 40°C to remove moisture and other impurities from the sample's surface and pores. Subsequently, the samples were placed in nitrogen for adsorption. The relative pressure was maintained within the range of 1.3×10^{-9} to 1 during the experimental procedure. Once adsorption equilibrium was reached, the volume of adsorbed gas at different relative pressures was measured to obtain the isotherm adsorption curve. The desorption isotherm curve was obtained by continuously decreasing the relative pressure to vacuum. After completion of the analysis, the Barrett–Joyner–Halenda (BJH) methods were implemented to elucidate the characteristics of the pore structure.

2.3.4. Dynamic Water Vapor Sorption (DVS). To replicate the moisture dispersion occurring within the pore structure of the cement paste, a dynamic water vapor sorption experiment in which the samples weighed approximately 25 mg was carried out using a Vapor Sorption Analyzer (model: TGA Q5000SA). The specimens were introduced into a controlled chamber where the RH was meticulously regulated. The RH levels ranged from 8% to 98% with intervals of 10% during both the adsorption and desorption phases, while maintaining a constant temperature of 20°C. The equilibration period for per step lasted for 8 hours.

3. Results

3.1. Carbonation Depth. The measurement of the carbonation depth provides a means to assess the degree of erosion inflicted upon the cement matrix by CO_2. The impact of various $Ca(NO_3)_2$ concentrations on the degree of carbonation depth is shown in Figure 2. Evidently, the $Ca(NO_3)_2$-treated concrete specimens exhibit reduced carbonation depth compared to the reference group at each designated carbonation duration. Specifically, in the sample containing 1% $Ca(NO_3)_2$, the carbonation depth at 28 days reduced from 15.2 mm to 12.2 mm; at 56 days, it reduced from 16.5 mm to 12.9 mm; at 90 days, it reduced from 17.8 mm to 13.4 mm; and at 180 days, it reduced from 19.2 mm to 16.0 mm. With the incorporation of 1% and 2% of $Ca(NO_3)_2$, a significant reduction in the initial stage (28 days) carbonation depth is observed. Subsequently, the rate of carbonation depth growth significantly decreases, and it is highly likely that even after 195 days, the carbonation depth will not exceed that of the control group. However, it is imperative to acknowledge that increasing the proportion of $Ca(NO_3)_2$ has not yielded the desired outcomes. In the case of the specimen infused with 3% $Ca(NO_3)_2$ following a storage of 180 days, the carbonation depth surpasses even that of the reference group.

3.2. Mechanical Strength and Cement Hydration. The evaluation of compressive strength at a hydration duration of 28 days is a widely applied method to characterize the early-stage hardening of cement pastes. Figure 3 illustrates the compressive strength behavior of samples with different amounts of $Ca(NO_3)_2$. The results showed that after $Ca(NO_3)_2$ was mixed into the concrete mixture, the strength of the matrix was improved to a certain extent, but the effect was not significant. Specifically, the compressive performance of the samples rises from 38.1 MPa to 40.9 MPa and 42.2 MPa when 1.0% and 2.0% $Ca(NO_3)_2$ are incorporated into the plain concrete, respectively. The compressive strength of samples containing 2% $Ca(NO_3)_2$ is higher than that of samples containing 1% $Ca(NO_3)_2$, which aligns with the experimental findings of Dorn et al. [16]. The incorporation of 1% and 2% $Ca(NO_3)_2$ resulted in a greater increase in compressive strength, and this is attributed to the involvement of $Ca(NO_3)_2$ in the hydration reactions within the cement matrix. The addition of $Ca(NO_3)_2$ facilitates the

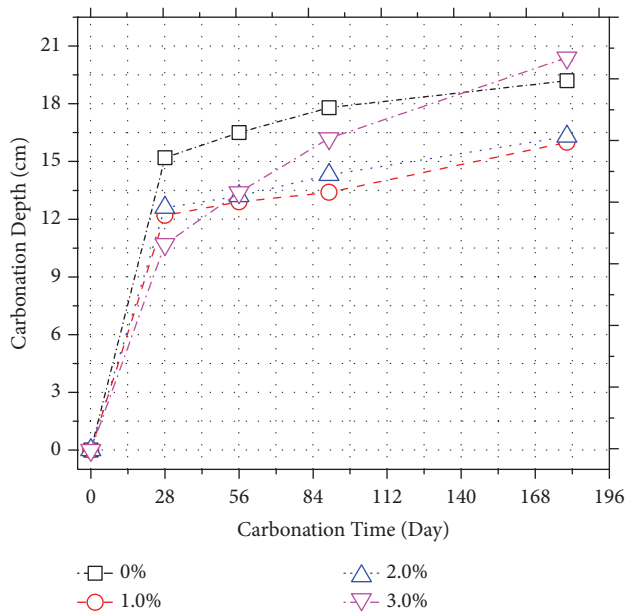

Figure 2: The carbonation depth of concrete incorporated with various amounts of $Ca(NO_3)_2$ admixture after 28, 56, 90, and 180 days of accelerated carbonation curing.

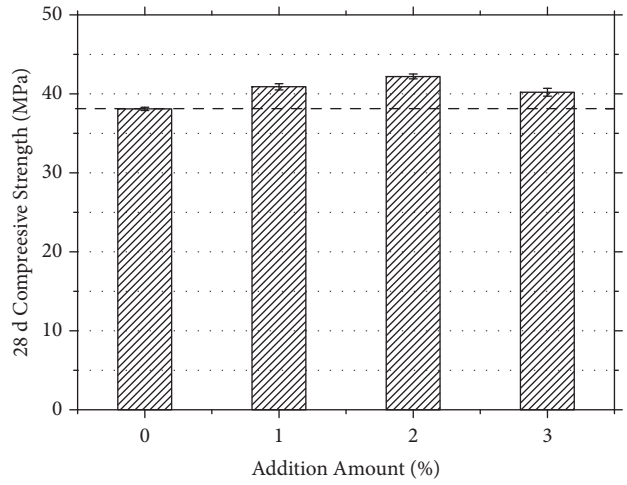

Figure 3: The compressive strength of samples incorporated with various amounts of $Ca(NO_3)_2$ admixtures after 28-day curing.

dissolution of gypsum, thereby increasing the formation of ettringite and NO_3-AFm, which ultimately leads to an increase in compressive strength. The thermodynamic calculations conducted by Balonis et al. corroborate the promotion of ettringite and NO_3-AFm formation upon the addition of $Ca(NO_3)_2$ [18]. However, when the dosage reaches 3.0%, the compressive performance decreases to 40.2 MPa. The excessive participation of $Ca(NO_3)_2$ in reactions promotes the abundant formation of AFm, which occupies the space intended for the hydration of C3S. This inhibits the hydration of C3S and reduces the generation of C-S-H, thereby partially offsetting the increase in compressive strength resulting from the significant formation of ettringite and AFm. These findings highlight the impact of different dosages on the compressive strength performance of the specimens.

The measurement of hydration heat serves as a crucial means to investigate the hydration process of cement. In Figure 4(a), the heat release rate of cement paste with different amounts of $Ca(NO_3)_2$ is depicted. The results demonstrate that the presence of $Ca(NO_3)_2$ reduces the induction period of cement hydration, as shown by the earlier appearance of the initial peak. Moreover, the maximum value of the groups containing $Ca(NO_3)_2$ surpasses that of the reference group, indicating an enhancement in compressive strength. Figure 4(b) displays the cumulative heat release profiles of samples with varying concentration. The cumulative exothermic heat liberation is closely linked to the degree of cement hydration, displaying a positive correlation that strengthens as the hydration process progresses. Prior to 40 hours, the cumulative heat release of the reference group lags that of the other samples, suggesting that $Ca(NO_3)_2$ promotes early hydration. After 150 hours, the total heat release of the sample incorporating various quantities of nitrate reaches 5000 J, indicating the progress of the hydration during the early stage.

3.3. XRD Analysis Results and Phase Composition. The promotion of $Ca(NO_3)_2$ on the hydration degree is presented in Section 3.2. There seems to be no positive influence on the extent of the late hydration process. To investigate such an effect, the pastes underwent X-ray diffraction (XRD) analysis and were characterized using the Rietveld method with TOPAS software. Figure 5 presents the XRD patterns of cement pastes with varying quantities of $Ca(NO_3)_2$ after 28d of hydration. It is obvious that no new phase appears when $Ca(NO_3)_2$ is incorporated. The addition of $Ca(NO_3)_2$ did not result in a significant change in the C3A content, which aligns with the conclusion drawn by Ye et al. [19]. Furthermore, each phase number was identified. As the main component generated during the whole hydration process, C-S-H constitutes a significant portion, approximately 60%, of the overall phase composition. Moreover, the amount of C-S-H reflects the extent of hydration. Compared with the reference paste, pastes with $Ca(NO_3)_2$ have less C-S-H. When the dosages of $Ca(NO_3)_2$ were 1%, 2%, and 3%, the C-S-H amount decreased from approximately 62% to 60%, 58%, and 58%, respectively. This phenomenon may be attributed to the extensive formation of AFm phases, which occupy a significant portion of the available space for C-S-H formation. $Ca(NO_3)_2$ exhibited a negative effect on the extent of the late hydration process, that is why the cumulative heat release was less than the reference paste in Section 3.2. In addition, more $Ca(OH)_2$ can be detected in pastes with $Ca(NO_3)_2$, and the reaction between $Ca(OH)_2$ and infiltrating CO_2 leads to a deceleration in the diffusion rate of CO_2 within the matrix, thereby explaining the reduction in carbonation depth.

3.4. Pore Structure (BET). As discussed, $Ca(NO_3)_2$ shows a slight influence on the cement hydration process. Specifically, $Ca(NO_3)_2$ slightly promotes the early

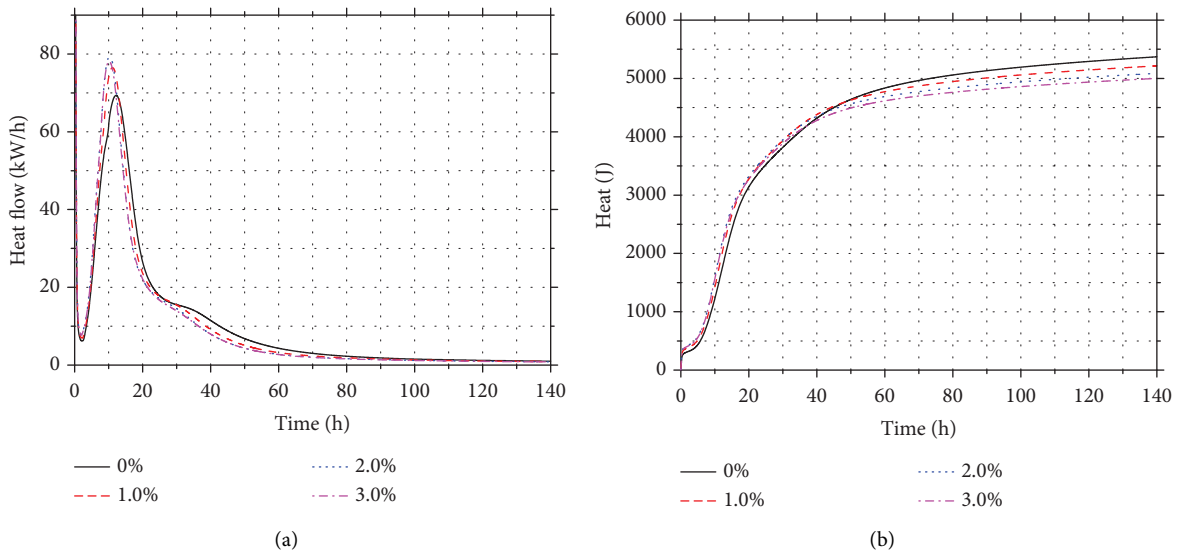

Figure 4: Effect of $Ca(NO_3)_2$ dosage on cement paste's calorimetric curve: (a) heat flow curve; (b) cumulative heat result.

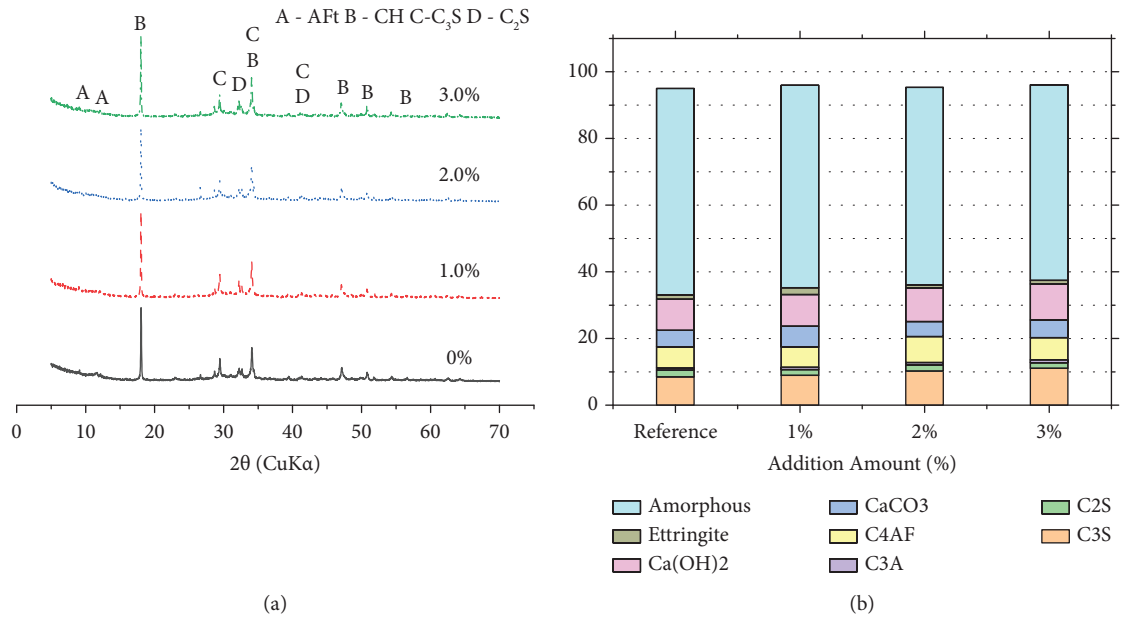

Figure 5: XRD results for samples with varying dosages of $Ca(NO_3)_2$: (a) XRD pattern; (b) phase number.

hydration stage. But it exhibited a slight negative effect on the extent of the late hydration process. Therefore, it seems that the hydration degree is not the main factor influencing the performance of concrete, including compressive strength and carbonation properties. The relationship of $Ca(NO_3)_2$ and pore structure was evaluated using the Brunauer–Emmett–Teller (BET) apparatus. The BET technique enables the determination of specific surface area and distribution of pore sizes, providing valuable insights into the pore structure properties of the cement paste samples.

The nitrogen sorption-desorption curves of cement paste samples with varying dosages of $Ca(NO_3)_2$ are depicted in Figure 6. At low to moderate relative pressures ($P/P_0 = 0{\sim}0.8$), with an increase in the content of $Ca(NO_3)_2$, the isotherm adsorption curves shift closer to the x-axis, indicating a weakening interaction between $Ca(NO_3)_2$ and N_2. At high relative pressures ($P/P_0 = 0.8{\sim}1.0$), a significant increase in N_2 adsorption is observed for all samples, indicating the presence of slit-like pores predominantly formed by the accumulation of lamellar particles (e.g., lamellar calcium hydroxide crystals). The adsorption capacity of N_2 and the area enclosed by the hysteresis loop decrease with an increase in the content of $Ca(NO_3)_2$. The inclusion of $Ca(NO_3)_2$ in the samples results in the formation of finer pores during the hydration process, accompanied by a reduction in the total number of pores. The changes in the shape of the hysteresis loop reflect an improvement in the pore structure, likely attributable to the

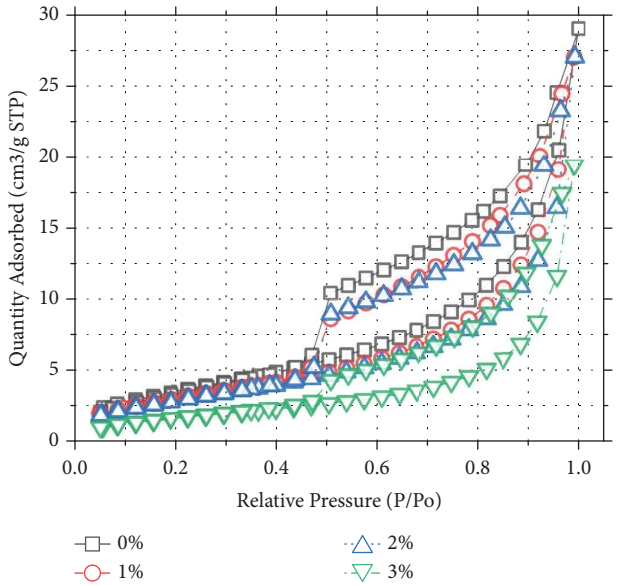

Figure 6: Nitrogen sorption and desorption curve for samples with varying amounts of $Ca(NO_3)_2$.

filling and refinement of pores by the formation of hydration products.

The application of the BJH method allowed for the quantification of pore characteristics, containing its cumulative volume and distribution, as illustrated in Figure 7. The results suggest that the samples incorporating $Ca(NO_3)_2$ exhibited reduced nitrogen gas absorption in comparison with the reference group. These findings suggest that the inclusion of $Ca(NO_3)_2$ influences the pore structure of the sample, resulting in altered nitrogen sorption behavior. Conventionally, reduced nitrogen adsorption is associated with diminished porosity and fewer interconnected pores. Moreover, specimens with higher $Ca(NO_3)_2$ concentrations demonstrate a propensity toward a further reduction in nitrogen adsorption, and this phenomenon can be ascribed to a diminishment in porosity and a decrease of connected pores. Furthermore, Figure 7(a) demonstrates that the cumulative pore volume of the $Ca(NO_3)_2$-treated sample exhibits a decreasing trend as the dosage increases. As the dosage of $Ca(NO_3)_2$ increases, the pore volume of small pore sizes (20–38 Å) decreases continuously. Within the intermediate pore size range (38–100 Å), the sample with 1% $Ca(NO_3)_2$ exhibits a slightly larger pore volume compared to the reference sample, while the sample with 3% $Ca(NO_3)_2$ has a slightly smaller pore volume than the reference sample. In contrast, the sample with 2% $Ca(NO_3)_2$ has a significantly smaller pore volume than the reference sample. Within the large pore size range (100–150 Å), the pore volume of the samples with 1% and 3% $Ca(NO_3)_2$ remains the same as the reference sample. However, the sample with 2% $Ca(NO_3)_2$ has a smaller pore volume than the reference sample. By calculating the total area underneath the pore volume curve, it can be observed that the cumulative pore volume decreases with an increasing dosage of $Ca(NO_3)_2$. The reduction in cumulative pore volume signifies an enhancement in the compactness of the cement matrix. Moreover, in the pore distribution curves as shown by Figure 7(b), there is a degradation observed in the peaks at approximately 3.5 nm for the samples incorporating $Ca(NO_3)_2$. This observation suggests that the presence of $Ca(NO_3)_2$ contributes to the densification of the pore characteristics in the cement paste.

Previous studies have reported that the correlation between relative pressure and adsorbed quantity can be applied to calculate the fractal factor of the pore structure in porous materials. This fractal factor provides valuable insights into the complexity and interconnectedness of the pore network within the cement paste. Table 3 shows that the $Ca(NO_3)_2$ addition declines the fractal dimension factor *Ds*, which decreases from 7.58958 to 7.16103, 6.97029, and 5.30373, respectively, when the $Ca(NO_3)_2$ amount changes from 0% to 3.0%. A higher *Ds* value represents the rougher and more irregular pore surface. Therefore, $Ca(NO_3)_2$ addition clearly decreases *Ds*, indicating a reduction in the complexity of the pore structure and a decrease in pore connectivity.

It has been confirmed that there are two types of calcium silicate hydrates with different density, which are produced during different stages of hydration process. The thermal analysis results of paste samples containing various amounts of nitrate are presented in Figure 8. These results can be utilized to determine the hydration level by quantifying the nonevaporable water content in comparison with the fully hydrated samples. Based on the findings by Taylor [20], it is established that completely hydrated cement pastes generally comprise around 23% nonevaporable water. By applying this information, the hydration degree can be computed, and the results are summarized in Table 4. The incorporation of $Ca(NO_3)_2$ reduces the degree of hydration in the cement matrix, and the higher the dosage of $Ca(NO_3)_2$, the greater the reduction in the degree of hydration. In accordance with Jennings' calcium silicate hydrate theory and previous calculations [21, 22], the ratio and surface area of LD C-S-H formed during the early stages of the hydration process were determined. The results presented in Table 4 indicate that the addition of $Ca(NO_3)_2$ leads to an increase in the content of LD C-S-H generated. However, the surface area of LD C-S-H exhibits an opposite trend, with a decrease of 12.26%, 18.14%, and 59.96% observed when 1.0%, 2.0%, and 3.0% $Ca(NO_3)_2$ were added, respectively. This is associated with the morphology of LD C-S-H, wherein if the formed LD C-S-H aggregates and forms clusters, it results in a reduction in specific surface area.

3.5. Moisture Diffusion (DVS). The transportation of gas molecules within porous materials is a complex process, wherein molecules of the medium can be adsorbed onto the pore surfaces of varying sizes under different applied relative pressures. The larger volume pores gradually undergo capillary condensation and multiple-layer adsorption, while the smaller holes gradually get filled with media molecules. The utilization of dynamic vapor sorption (DVS) is an efficient method for evaluating water vapor transport in porous materials. In the DVS measurement technique, the moisture content of the sample is considered as a function of water activity and adsorption kinetics, using adsorption

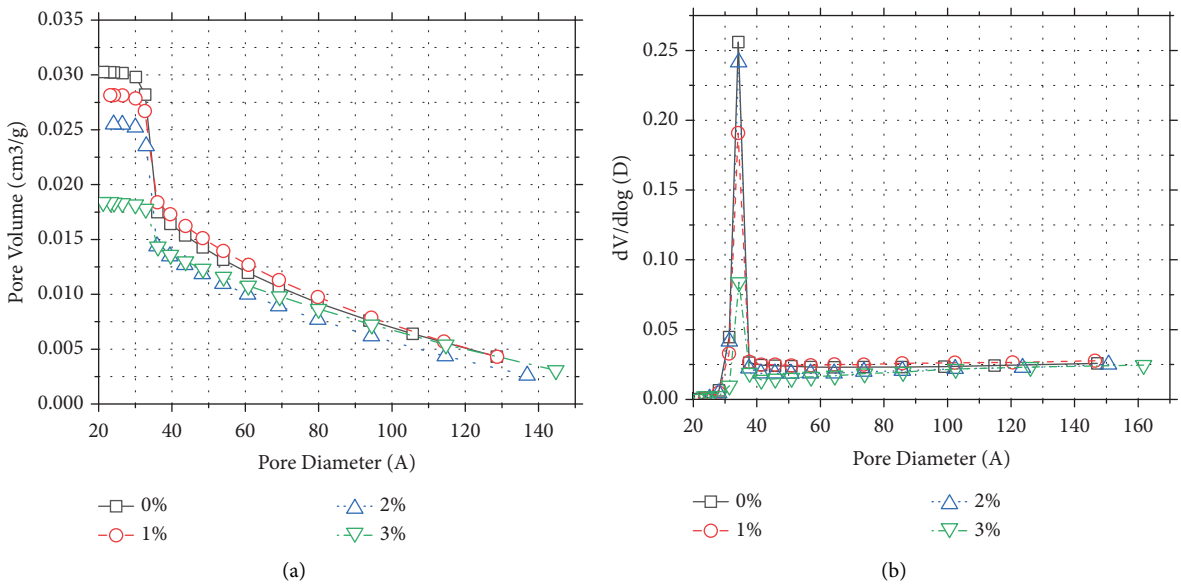

Figure 7: Results from BJH method: (a) cumulative pore volume curve; (b) pore size distribution result.

Table 3: Pore structure and fractal parameters calculated from nitrogen sorption isotherm.

Calcium nitrite amount (%)	0	1.0	2.0	3.0
Cumulative volume of pores (cm^3/g)	0.030265	0.028156	0.025498	0.018405
Average pore diameter (Å)	55.047	48.385	61.021	51.872
Csp	1.52986	1.38701	1.32343	0.76791
Ds	7.58958	7.16103	6.97029	5.30373

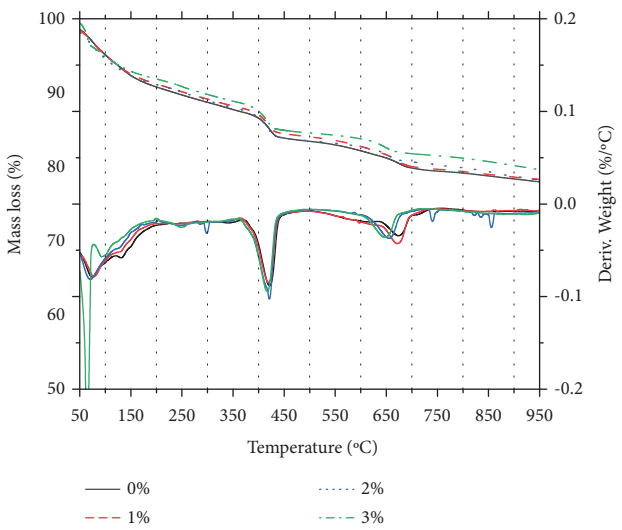

Figure 8: Thermal analysis of cement pastes incorporated with varying proportions of nitrate at the stage of 28-d hydration.

Table 4: Chemical bound water and C-S-H gel characteristics parameter in cement pastes.

Calcium nitrite amount (%)	0	1.0	2.0	3.0
Nonevaporable water percent (%)	17.10	16.75	16.43	15.35
Hydration degree*[a] (%)	74.33	72.823	71.41	66.72
Amount of C-S-H generation (%)	61.96	60.92	59.25	58.66
BET surface area (m^2/g)	13.4723	11.6319	10.9043	6.602
Ratio of LD C-S-H (%)	32.17	32.61	33.01	34.38
Surface area of LD C-S-H (m^2/g)	95.70	83.96	80.466	47.456

[a]From Taylor, fully hydrated cement pastes typically contain about 23% of nonevaporable water.

isotherms to investigate water adsorption properties. These water absorption characteristics are determined by the changes in sample weight during humidity absorption or diffusion processes. Figure 9 presents the weight variation of cement pastes containing $Ca(NO_3)_2$ under varying humidity conditions during vapor sorption measurements. Based on the weight response data, the hysteresis loop is calculated and depicted in Figure 10. It is observed that the highest hysteresis content is attained at a humidity level of 75% for all samples. Furthermore, the hysteresis values of the samples incorporating $Ca(NO_3)_2$ are significantly lower than those of the reference. Notably, the hysteresis content of the samples with 1.0% and 2.0% $Ca(NO_3)_2$ is lower than that of the reference, while the content of the paste with 3.0% $Ca(NO_3)_2$ is higher than that of the reference within the range of 55% to 85% relative humidity. This phenomenon aligns with the carbonation depth process and will be further discussed in Section 4.

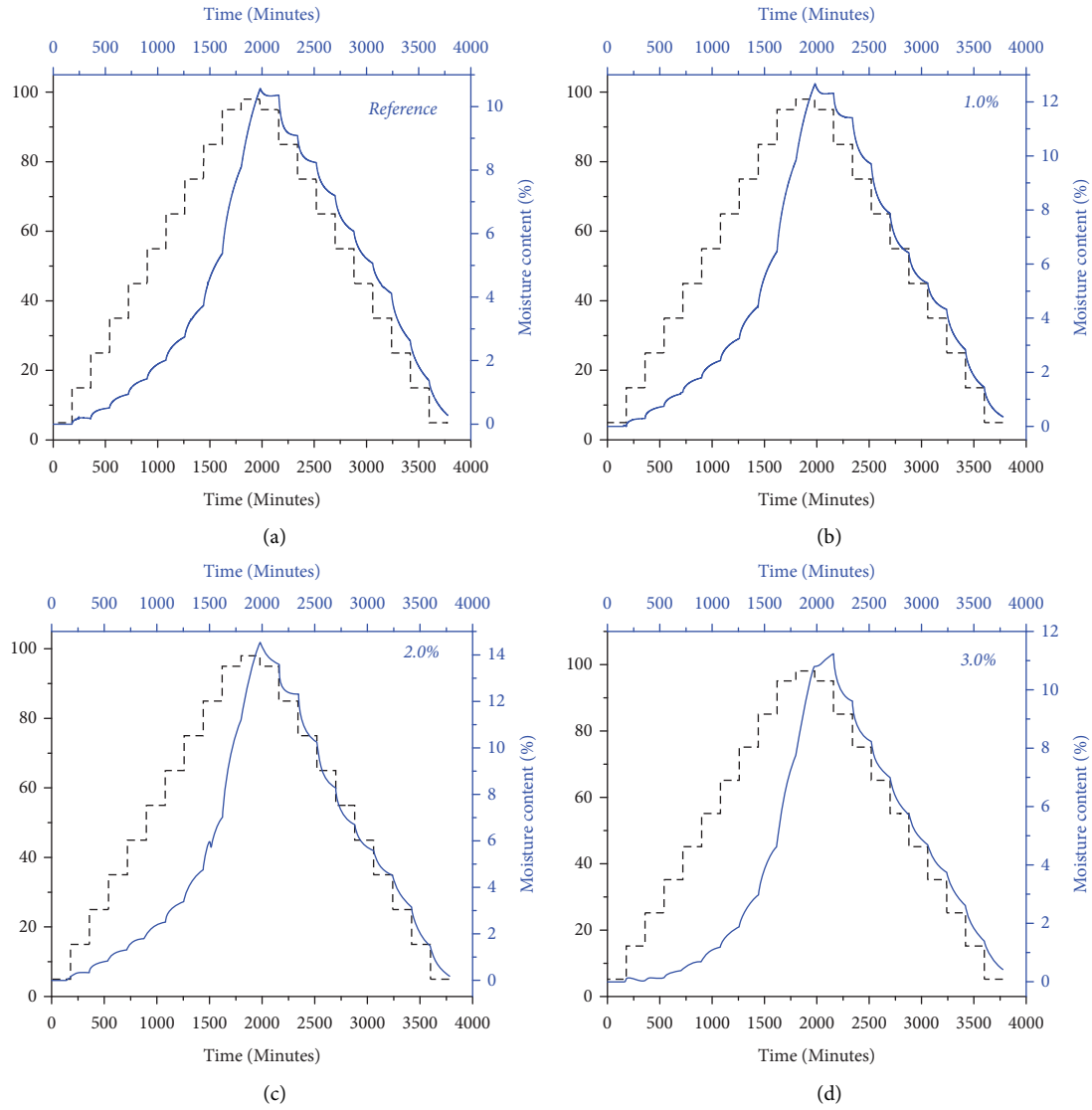

Figure 9: Dynamic vapor isothermal curve of cement paste containing (a) 0%, (b) 1.0%, (c) 2.0%, and (d) 3.0% chemical admixture. The black and blue lines represent relative humidity and moisture content shown on the primary and secondary y-axis.

4. Discussion

4.1. $Ca(NO_3)_2$ Improves Carbonation Resistance. It should be noted that the addition of $Ca(NO_3)_2$ in an amount smaller than 3.0% can improve the carbonation durability of cementitious materials. The carbonation process of cementitious material mainly relates to the microstructure, including the hydration products, pore structure, and the pore solution. $Ca(NO_3)_2$ exhibits little positive effect on the hydration of cement. However, there is no C-S-H growth because of the addition of $Ca(NO_3)_2$, and the formation amount of calcium hydroxide improves, thereby sustaining the alkaline environment and retarding the neutralization of cementitious materials. As detected by BET, the pore structure reveals a linear negative correlation between pore volume and average pore size with the dosage of $Ca(NO_3)_2$, which contradicts the relationship between carbonation depth of cement and the amount of $Ca(NO_3)_2$ used. When different dosages of $Ca(NO_3)_2$ admixture are added to cementitious materials, the pore structure undergoes refinement, leading to a decrease in pore density. Consequently, the flow of carbon dioxide gas into the cementitious material is restricted. Furthermore, the interconnectivity of pores is also a crucial factor that influences the carbonation resistance of cementitious materials. The nitrogen sorption and desorption curve indicate that the pore connectivity in cementitious materials is declined by the incorporation of $Ca(NO_3)_2$, which further leads to a reduction in the diffusion of carbon dioxide. Regarding the nitrogen sorption and desorption curves, the curve corresponding to the reference group displays the biggest total volume adsorbed in all samples (around 29 cm^3/g). Moreover, the adsorbed volume in the reference group, which is around 11 cm^3/g, is higher than that of samples with different dosages of $Ca(NO_3)_2$ at a relative pressure value of 0.5. However, the addition of 3.0% $Ca(NO_3)_2$ can reduce the carbon dioxide resistance of cementitious materials in 90 days, which is also related to the pore connectivity. Justnes's experimental studies [23] have

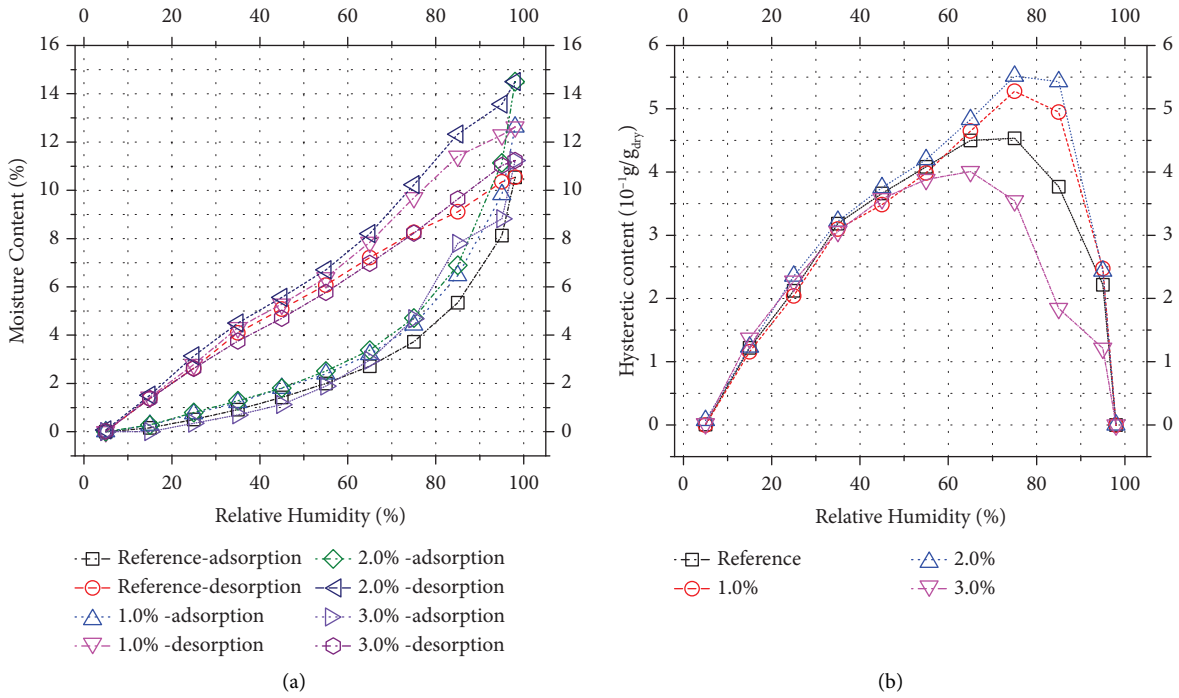

FIGURE 10: (a) Effect of different amounts of $Ca(NO_3)_2$ on moisture content adsorbed by cement paste; (b) the hysteretic curve recalculated by moisture content at the same humidity. The adsorption and desorption are fitted by the dashed lines.

shown that the steady-state migration coefficient D_m when 2.0% $Ca(NO_3)_2$ is added into the cementitious materials doubles than those of the reference sample. The D_m is tightly related to the porosity and pore connectivity. More specifically, the higher porosity and connectivity result in a higher value of D_m. Due to the fact that the addition of different amounts of $Ca(NO_3)_2$ decreases the porosity, it can be inferred that the D_m can be reduced by adding 3.0% $Ca(NO_3)_2$, so the pore connectivity of cementitious materials with 3.0% $Ca(NO_3)_2$ increases. Accordingly, the gas migration coefficient of cementitious material with a higher amount of $Ca(NO_3)_2$ can be reduced.

According to the fractal scaling law, a bundle of tortuous pores is assumed in cement-based material, and the effective permeability k can be derived according to the Hagen–Poiseuille equation and Darcy's law, as shown in the following:

$$k = \frac{(\pi D_s)^{(1-D_T)/2}\left[4(2-D_s)\right]^{(1+D_T)/2}}{128(3+D_T-D_s)}\left(\frac{D}{1-\phi}\right)^{(1+D_T)/2} d_{\max}^2, \quad (1)$$

where D_T is the tortuosity fractal dimension, ϕ represents the porosity, and $d_{\max}$ represents the maximum pore size.

Tortuosity fractal dimension is related to connectivity as shown in the previous study [24]. Based on the reference value, that of the plain cementitious material sample is estimated at 1.0 and shows more connected pore structure. In addition, the pore system with micrometer scale shows disconnected characteristics and the gas diffusion process is determined by the connected capillary pores based on the common value 500 nm [25]. The results of the average pore diameter tested by BET in Table 5 show that the lower tortuosity fractal dimension and the porosity have great effects on the permeability of concrete. The moisture diffusion experiments using DVS measurement show that the addition of 3.0% $Ca(NO_3)_2$ increases the pore system connection when the hysteretic curve presents higher content. On the other hand, when the relative humidity is more than 55%, a water layer forms on the surface of the pore system and the amount of moisture in and out of the sample with 3.0% $Ca(NO_3)_2$ is smaller than that of other samples, which confirms the fact that the higher amount of $Ca(NO_3)_2$ improves the connectivity of cementitious materials.

4.2. The Modification Mechanism on Microstructure by $Ca(NO_3)_2$. The microstructure change of cementitious materials is tightly related to the cement hydration process. It has been observed in calorimetric measurements that the addition of $Ca(NO_3)_2$ will increase the hydration peak and the hydration flow of the acceleration period, but the hydration degree after the deceleration period is not extended. Based on the calculation of LD C-S-H, the ratio of LD C-S-H is observably increased with the additional amount of calcium nitrate, while the surface area of LD C-S-H decreases. It should be noted that the low-density C-S-H generated in the period of early hydration includes the induction and acceleration period. The increased amount of LD C-S-H permits greater ion diffusion into the pore solution, so the reaction of hydration products gets enhanced. The research findings by Dorn et al. [16] demonstrate that the addition of $Ca(NO_3)_2$ significantly increases the

Table 5: The gas permeability characteristics of cement pastes mixed with $Ca(NO_3)_2$.

$Ca(NO_3)_2$ amount (%)	D_s	D_T	d_{max}	Porosity (%)	Permeability (10^{-16} m^2)
0	7.58958	1.05	500.00	0.030265	3.317
0.6	7.16103	1.10	519.16	0.028156	3.594
0.9	6.97029	1.30	487.94	0.025498	3.562
1.2	5.30373	1.00	534.41	0.018405	2.957

concentration of Ca^{2+} in the pore solution of cement paste within the first hour of hydration. In a previous study [21], the hydration rate of the acceleration period is linearly dependent on the addition of a temperature-rising inhibitor, which proves that the rate of acceleration period is primarily governed by the growth of C-S-H, which serves as the limiting step. However, the study also seems to show that the cement hydration accelerated by alkali salts results from the ion motility and the changes of the diffusion characteristics. Taking the development of calcium silicate hydrates and the influence of alkali into consideration [22], the incorporation of calcium ions plays an important role in the growing hydrate, which determines the hydration rate [26], but the presence of anion shows the charge shielding, which means that a single calcium ion incorporated into the hydrates causes the two plus surface charge. It can be inferred that mobile anions in the close vicinity are needed to minimize the free energy of a hypothetical positively charged transition state. Therefore, the addition of more $Ca(NO_3)_2$, ion motility, and the changes in the diffusion characteristics result in the change of the surface area and the charge state of hydrates. The mechanism is consistent with the results of pore structure and the density of low-density calcium silicate hydrates, which can also be used to analyze STXM and NMR results of previous studies [27–29].

5. Conclusions

In this study, the influence of $Ca(NO_3)_2$ on the carbonation properties of cement-based materials was comprehensively examined utilizing isothermal conduction calorimetry, XRD, BET analysis, and water vapor sorption. From the conducted analyses, the following pivotal findings can be deduced:

(1) The incorporation of $Ca(NO_3)_2$ enhances the carbonation resistance of cementitious materials, provided that the dosage is lower than 3.0%

(2) The carbonation resistance improvement of $Ca(NO_3)_2$ addition results from the increase of small pores and the change of tortuosity, as the lower tortuosity fractal dimension and porosity have obvious effects on the permeability of concrete

(3) The moisture diffusion experiments have also shown that the addition of 3.0% $Ca(NO_3)_2$ shows a more connected pore system when the hysteretic curve presents higher content, which confirms the fact that the higher amount of $Ca(NO_3)_2$ improves the connectivity of cementitious materials

(4) The modification mechanism on microstructure by $Ca(NO_3)_2$ is mainly attributed to the fact that ion motility and the changes of the diffusion characteristics result in the change of the surface area and the charge state of hydrates

Data Availability

The datasets used and/or analyzed during the current study are available from the corresponding author upon reasonable request.

Disclosure

A preprint has previously been published [Hao Zhang, et al. 2023], which has been listed in the references list number [30, 31].

Conflicts of Interest

The authors declare that they have no conflicts of interest that could have appeared to influence the work reported in this study.

Authors' Contributions

Hao Zhang conceptualized the study, proposed the methodology, performed investigation, wrote the original draft, and provided funding acquisition. Luqing Cheng proposed the methodology, performed investigation, and wrote, reviewed, and edited the manuscript. Jingsheng Pan conceptualized the study, performed investigation, and reviewed and edited the manuscript. Guodong Xu provided resources, conceptualized the study, and performed investigation. Xuyan Shen proposed the methodology, performed investigation, and reviewed and edited the manuscript. Song Mu proposed the methodology, performed investigation, reviewed and edited the manuscript, and provided funding acquisition. Jingshun Cai provided resources, proposed the methodology, performed investigation, and reviewed and edited the manuscript. Jianzhong Liu performed investigation and reviewed and edited the manuscript. Jinxiang Hong reviewed and edited the manuscript and performed project administration. Zhiqiang Yang, Zhonglai Yi, Huajian Li, and Ying Zhou performed investigation and reviewed and edited the manuscript. Jingsheng Pan, Zhiqiang Yang, Zhonglai Yi, and Huajian Li contributed to the process of responding to the comments of the reviewers and revising the manuscript, and they provided a wealth of experience and intellectual achievements. The authors declare that they agree to be authors and acknowledge their scientific contributions to this manuscript. The authors confirm that this is the final

authorship and that anyone else who contributed has been acknowledged with their permission.

Acknowledgments

The authors wish to acknowledge financial support from the Science and Technology Program Special Fund of Jiangsu Province (Frontier Leading Technology Basic Research) Major projects, China (No. BK20222004); the National Key R&D Program of China, China (No. 2021YFB2601000); the National Natural Science Foundation of China (No. 52108217); the Natural Science Foundation of Jiangsu Province (No. BK20210954); and National Key Laboratory of High-speed Railway Track System (China Railway Research Institute Group Co., LTD.), China (No. 2023YJ376-1).

References

[1] M. Venkata Rao, R. Sivagamasundari, and T. Vamsi Nagaraju, "Achieving strength and sustainability in ternary blended Concrete: leveraging industrial and agricultural By-Products with controlled Nano-SiO2 content," *Cleaner Materials*, vol. 9, Article ID 100198, 2023.

[2] P. Van den Heede and N. De Belie, "A service life based global warming potential for high-volume fly ash concrete exposed to carbonation," *Construction and Building Materials*, vol. 55, pp. 183–193, 2014.

[3] L. J. Parrott and D. C. Killoh, "Carbonation in a 36 year old, in-situ concrete," *Cement and Concrete Research*, vol. 19, no. 4, pp. 649–656, 1989.

[4] N. De Belie and S. Lammertijn, "Gas transport and carbonation in high-volume fly ash concrete versus age at testing," *International Symposium Non-Traditional Cement & Concrete III*, Brno, Czech Republic, pp. 76–85, 2008.

[5] A. Steffens, D. Dinkler, and H. Ahrens, "Modeling carbonation for corrosion risk prediction of concrete structures," *Cement and Concrete Research*, vol. 32, no. 6, pp. 935–941, 2002.

[6] S. von Greve-Dierfeld, B. Lothenbach, A. Vollpracht et al., "Understanding the carbonation of concrete with supplementary cementitious materials: a critical review by RILEM TC 281-CCC," *Materials and Structures*, vol. 53, no. 6, p. 136, 2020.

[7] P. Van den Heede, M. De Schepper, and N. De Belie, "Accelerated and natural carbonation of concrete with high volumes of fly ash: chemical, mineralogical and microstructural effects," *Royal Society Open Science*, vol. 6, no. 1, Article ID 181665, 2019.

[8] P. Liu, Z. Yu, and Y. Chen, "Carbonation depth model and carbonated acceleration rate of concrete under different environment," *Cement and Concrete Composites*, vol. 114, Article ID 103736, 2020.

[9] N. De Belie, J. Kratky, and S. Van Vlierberghe, "Influence of pozzolans and slag on the microstructure of partially carbonated cement paste by means of water vapour and nitrogen sorption experiments and BET calculations," *Cement and Concrete Research*, vol. 40, no. 12, pp. 1723–1733, 2010.

[10] S. Lammertijn and N. De Belie, "Porosity, gas permeability, carbonation and their interaction in high-volume fly ash concrete," *Magazine of Concrete Research*, vol. 60, no. 7, pp. 535–545, 2008.

[11] N. I. Fattuhi, "Concrete carbonation as influenced by curing regime," *Cement and Concrete Research*, vol. 18, no. 3, pp. 426–430, 1988.

[12] Y. Lo and H. M. Lee, "Curing effects on carbonation of concrete using a phenolphthalein indicator and Fourier-transform infrared spectroscopy," *Building and Environment*, vol. 37, no. 5, pp. 507–514, 2002.

[13] J. P. Balayssac, C. H. Détriché, and J. Grandet, "Effects of curing upon carbonation of concrete," *Construction and Building Materials*, vol. 9, no. 2, pp. 91–95, 1995.

[14] P. Barnes and J. Bensted, *Structure and Performance of Cements*, CRC Press, Boca Raton, FL, USA, 2002.

[15] H. Justnes and E. C. Nygaard, "Changes in the microstructure of cement paste and concrete due to calcium nitrate addition," *Special Publication*, vol. 173, pp. 657–672, 1997.

[16] T. Dorn, T. Hirsch, and D. Stephan, "Working mechanism of calcium nitrate as an accelerator for Portland cement hydration," *Journal of the American Ceramic Society*, vol. 106, no. 1, pp. 752–766, 2023.

[17] T. V. Nagaraju, S. B. Malegole, B. Chaudhary, and G. Ravindran, "Assessment of environmental impact of aquaculture ponds in the western delta region of Andhra Pradesh," *Sustainability*, vol. 14, no. 20, p. 13035, 2022.

[18] M. Balonis, M. Medala, and F. P. Glasser, "Influence of calcium nitrate and nitrite on the constitution of AFm and AFt cement hydrates," *Advances in Cement Research*, vol. 23, no. 3, pp. 129–143, 2011.

[19] S. Ye, P. Feng, Y. Liu, J. Liu, and J. W. Bullard, "Dissolution and early hydration of tricalcium aluminate in aqueous sulfate solutions," *Cement and Concrete Research*, vol. 137, Article ID 106191, 2020.

[20] H. F. Taylor, *Cement Chemistry*, Thomas Telford London, London, UK, 1997.

[21] H. Zhang, L. Li, P. Feng, W. Wang, Q. Tian, and J. Liu, "Impact of temperature rising inhibitor on hydration kinetics of cement paste and its mechanism," *Cement and Concrete Composites*, vol. 93, pp. 289–300, 2018.

[22] H. Taylor, P. Barret, P. W. Brown et al., "The hydration of tricalcium silicate: rilem committee 68-mmh, task group 3," *Materials and Structures*, vol. 17, no. 6, pp. 457–468, 1984.

[23] H. Justnes, A. Thys, F. Vanparijs, and D. Van Gemert, "Porosity and diffusivity of concrete with long-term compressive strength increase due to addition of the set accelerator Calcium Nitrate," *9th international conference on durability of building materials and components*, Brisbane, Australia, 2002.

[24] B. Yu and P. Cheng, "A fractal permeability model for bi-dispersed porous media," *International Journal of Heat and Mass Transfer*, vol. 45, no. 14, pp. 2983–2993, 2002.

[25] T. C. Powers and T. L. Brownyard, "Studies of the physical properties of hardened portland cement paste," *Journal Proceedings*, vol. 43, no. 9, 1946.

[26] R. Kondo, M. Daimon, E. Sakai, and H. Ushiyama, "Influence of inorganic salts on the hydration of tricalcium silicate," *Journal of Biochemical Toxicology*, vol. 27, no. 1, pp. 191–197, 1977.

[27] Q. Li, Y. Wang, G. Geng et al., "Microstructural study of hydration of C3S in the presence of calcium nitrate using scanning transmission X-ray microscopy (STXM)," *Journal of Nanomaterials*, vol. 2020, Article ID 8419130, 9 pages, 2020.

[28] Q. Li, Y. Ge, G. Geng, S. Bae, and P. J. Monteiro, "CaCl2-accelerated hydration of tricalcium silicate: a STXM study combined with 29Si MAS NMR," *Journal of Nanomaterials*, vol. 2015, no. 1, Article ID 215371, 10 pages, 2015.

[29] Z. Zheng, Y. Li, Z. Zhang, and X. Ma, "The impacts of sodium nitrate on hydration and microstructure of Portland cement and the leaching behavior of Sr2+," *Journal of Hazardous Materials*, vol. 388, Article ID 121805, 2020.

[30] H. Zhang, X. Shen, S. Mu, J. Cai, J. Liu, and J. Hong, "Carbonization properties of cement-based materials affected by calcium nitrite," https://papers.ssrn.com/sol3/papers.cfm?abstract_id=4365799.

[31] H. Zhang, L. Chen, S. Mu, J. Cai, J. Liu, and J. Hong, "Effects of urea on carbonation properties and microstructure of cementitious materials," *Materials Today Communications*, vol. 36, Article ID 106570, 2023.